IEEE Access
Multidisciplinary | Rapid Review | Open Access Journal

Received May 13, 2020, accepted May 28, 2020, date of publication June 5, 2020, date of current version June 17, 2020.

Digital Object Identifier 10.1109/ACCESS.2020.3000247

Coordinated Fuzzy-Based Low-Voltage Ride-Through Control for PMSG Wind Turbines and Energy Storage Systems

CHUNGHUN KIM[1], (Member, IEEE), AND WONHEE KIM[2], (Member, IEEE)
[1]Department of AI Electrical Engineering, Pai Chai University, Daejeon 35345, South Korea
[2]School of Energy Systems Engineering, Chung-Ang University, Seoul 06974, South Korea

Corresponding author: Wonhee Kim (whkim79@cau.ac.kr)

This work was supported in part by the Energy Cloud Research and Development Program through the National Research Foundation of Korea (NRF) funded by the Ministry of Science and ICT under Grant NRF-2019M3F2A1073313 and in part by the Basic Science Research Program through the National Research Foundation of Korea (NRF) funded by the Ministry of Education (2019R1I1A1A01063281).

ABSTRACT Coordinated control methods involving a wind turbine (WT) and an energy storage system (ESS) have been proposed to meet several objectives, such as smoothing wind power (WP) fluctuations, shaving peaks, enabling power scheduling, and allowing low-voltage ride-through (LVRT). LVRT requirement is defined by grid operators, and it should be satisfied whenever grid faults occur. Several methodologies have been proposed for the LVRT both with or without the use of an ESS. Furthermore, using an ESS is more advantageous for several WP applications. By using an ESS, WTs can be operated in a more economic and reliable way. However, the installation cost of an ESS is high and it has operation range constraints for charging and discharging. Moreover, the WT operation condition and ESS state-of-charge (SoC) can be different when a grid fault occurs. Therefore, it is necessary to coordinate both units, WT and ESS, for reliable and economic operation during a grid fault. Thus, we propose a coordinated fuzzy-based LVRT method that considers the different operation conditions of a WT and an ESS. From the proposed method, the effective reference powers of a WT and an ESS are evaluated by considering the rotor speed and SoC in the fuzzy control algorithm. The effectiveness of the proposed method is validated by considering two case studies on ESS SoC and WT rotor speed violations.

INDEX TERMS Coordinated controller, DC link regulation, energy storage system, fuzzy-logic controller, inertial response, low-voltage ride-through, rotor speed violation.

NOMENCLATURE

- ESS: Energy storage system
- LVRT: Low-voltage ride-through
- MPPT: Maximum power point tracking
- MSC: Machine-side converter
- GSC: Grid-side converter
- PCC: Point of common coupling
- PMSG: Permanent magnet synchronous generator
- SoC: State-of-charge
- WPS: Wind power system
- WT: Wind turbine

I. INTRODUCTION

Generally, as wind power (WP) increases in proportion to the total grid power, several issues related to the economic and reliable operation of an integrated power grid become apparent. There are several types of wind power systems (WPSs), and the permanent magnet synchronous generator (PMSG) wind turbines (WTs) are one of the popular WPSs. The doubly fed induction generator (DFIG) WT is also a popular WPS along with the variable speed WT (VSWT); however, PMSG WTs have several advantages over DFIG WTs. The most advantageous feature of a PMSG WT is its large operation range as it fully uses the power converters of machine-side converter (MSC) and grid-side converter (GSC) [1], [2]. As the size of a WT grows, this advanced power converter control method affects the economy and reliability of its operation significantly. From the converter control methods, WPS can produce maximum available power [3] and control the active and reactive powers according to certain operating conditions. As the use of WP in the power networks increases, its impact on grid operations becomes more significant [4]. For the reliable and economic operation of a WPS, it should

The associate editor coordinating the review of this manuscript and approving it for publication was Manoj Datta.

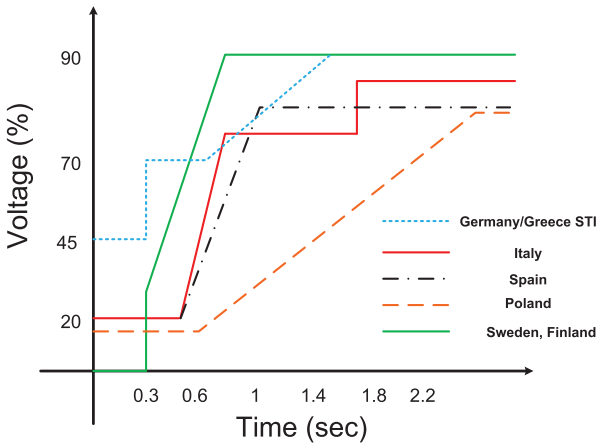

FIGURE 1. Limit curves for voltage to allow generator disconnection.

switch between maximum power point tracking (MPPT) and grid support operations [5], [6]. Grid operators require WTs to remain connected to a grid when the grid voltage sags, which is important for grid integration of a WPS. As shown in Fig. 1, grid operators have their own grid codes, which define grid requirements differently in the case of a grid voltage event. The duration of a forced connection according to the voltage sag profile varies based on the characteristics of the WPS [7]. The grid characteristics can be changed as the WPS penetration level increases, and consequently the grid code is redefined.

Various methods have been proposed for LVRT control. A proportional-integral (PI) current controller for DC-link voltage regulation using current feed-forward methods was proposed for better transient response. Furthermore, the impact of unbalanced voltage sags on the controller performance was studied [8]. A feedback linearization controller was proposed in [9] for the nonlinear control of the GSC in a PMSG. Using this controller, the performance of GSC current control during voltage sag could be improved by maintaining its current rate in a given range. This method is complex to implement; thus, feedback linearization was implemented using sliding mode control [10]. A sliding mode control algorithm was applied to GSC control for regulating DC-link voltage. This results in a better performance as compared to linear controller because DC-link voltage dynamics are nonlinear and the GSC follows nonlinearity in its switching operation. A combined control for pitch and MSC was proposed in [11]. The researchers used a breaking resistor to ensure that the WPS does not breach the current limit or rotor speed limit during LVRT. In some previous studies [12], [13], MSC was used to handle DC-link regulation instead of a GSC during grid fault, because the latter should control its active and reactive power supports during a grid fault. Thus, changing the roles of GSC and MSC in terms of DC-link regulation may be more advantageous. In this case, the rotor speed can be increased by storing the remaining mechanical power as WT inertia, which is similar to that observed during grid fault. In [12], a feedback linearization method was designed for MSC control. For LVRT operation, some researchers considered methods that involve additional device installation. In recent years, energy storage systems (ESSs) have been connected to WPSs for achieving many objectives by modulating the wind power [5]. This helps the integration of WP into the grid and also makes the WPS more cost-efficient. According to one strategy, an ESS can help a WT as an LVRT solution. This methodology resulted in a better LVRT response as compared to that when using converter control. In addition, an ESS stores the power instead of just dissipating it. In [14], the researchers proposed an energy storage-based LVRT method with direct-drive WPS with no power control capability. In [15], [16], LVRT methods were proposed using an ESS to improve the LVRT response. In these cases, an ESS was interconnected with wind farms to help voltage restoration at the point of common coupling (PCC). In [17], for better reactive power support during grid faults, the optimal reactive control method was proposed for production cost minimization.

In this study, we propose a coordinated fuzzy-based LVRT method that considers the inertial response capability of a WT and an ESS SoC. Previous studies have focused on the ESS LVRT control method, which regulates DC-link voltage during a grid fault. However, an ESS can have different SoC values when the grid fault occurs. When the ESS approaches its SoC limit before the grid fault is cleared, the DC-link voltage can vary significantly. Thus, it is important to coordinate the LVRT control between the WT and the ESS during a grid fault. We formulate the fuzzy-based LVRT control method by considering the LVRT capabilities of the WT and the ESS. In the proposed method, the LVRT control is properly divided between these devices. Thus, LVRT control is successfully achieved without violating the device constraints. When implementing the proposed method, the required reserve capacity of the ESS can be significantly reduced, because the inertial response of the WT is determined using the maximum rotor speed limit. This inertial response capability differs according to the rotor speed at the time of a grid fault. To validate the effectiveness of the proposed method, case studies on SoC limit problem and rotor speed violation during a grid fault are considered in MATLAB/Simulink SimPowerSystems considering topological circuit model. We also validated the proposed method in real time simulation in Scalexio which is developed by DSPACE. From the simulation results, the proposed method effectively achieve reliable operation without violating the constraints. Compared to the previous works of LVRT, the benefits of the proposed method can be described as follows.

- The proposed method can enhance LVRT response guaranteeing the stability.
- The proposed fuzzy logic control method is easy to be applied to physical system since it uses measurement data from a WT and an ESS.
- The proposed method can effectively avoid the stability problem due to inappropriate control gains of a WT and an ESS for dc link voltage regulation.

II. PMSG WPS

In this section, we discuss the mechanical power of the WT, MSC and GSC models, DC-link voltage and ESS dynamics.

A. MECHANICAL POWER OF WTs

The mechanical power of a WT can be described by defining the power coefficient, C_p which is modulated by the rotor speed, pitch angle, β. The tip speed ratio, λ, can be modulated by controlling the rotor speed and pitch angle; and when the tip speed ratio maintains its optimal value, the maximum available mechanical power of the WT can be achieved using the following equation [11]:

$$\begin{aligned} P_t &= \frac{1}{2}\rho A C_p(\lambda, \beta) v_{wind}^3, \\ \lambda &= \frac{\omega_m R}{v_{wind}}, \end{aligned} \tag{1}$$

where ρ denotes the air density and A is the blade-swept area that increases with the increase in the rotor radius, R. C_p is a function of the pitch angle and tip speed ratio, and the parameters of this function are obtained from the WT experimental data. v_{wind} is the wind velocity, which affects the mechanical power by affecting the cubic value and tip speed ratio. Therefore, the power coefficient indicates the ratio of the electric power produced by the WT to the total power available from the wind speed. Its theoretical limit is mathematically defined to be 0.5926. The achievable value is less than this limit because of the loss experienced by mechanical systems in a WT. Therefore, we used a maximum C_p value of 0.5 in this study.

B. MSC MODEL

To describe MSC power production, PMSG electrical equations involving the voltage and current are used; the electrical and mechanical torque of the MSC can be calculated from the following equations [13]:

$$\begin{aligned} v_{dg} &= R_s i_{dg} + L_s \frac{di_{dg}}{dt} - \omega_s L_s i_{qg}, \\ v_{qg} &= R_s i_{qg} + L_s \frac{di_{qg}}{dt} + \omega_s L_s i_{qg} + \omega_s \lambda_f, \\ T_e &= \frac{3}{2} p \lambda_f i_{qg}, \\ T_m - T_e &= J \frac{d\omega_m}{dt}, \end{aligned} \tag{2}$$

where v_{dg} and v_{qg} denote the stator voltages of the PMSG, and i_{dg} and i_{qg} denote the stator currents. L_s and R_s denote the stator inductance and resistance, respectively, and ω_s denotes the rotor flux electrical speed. ω_m denotes the speed of the PMSG mechanical rotor; λ_f denotes the rotor flux; and p denotes the machine pole pairs, which represent the ratio of electrical speed to mechanical speed. T_e and T_m denote the electromagnetic and mechanical torques, respectively. J denotes the rotor inertia. The rotor speed can be calculated using equations that describe the relationship between T_e, T_m, and J. A surface-mounted PMSG with similar d- and q-axes inductances was used in this investigation. A reluctance torque, which is induced by the difference between these inductances, does not exist. Therefore, we can use Eq. (2) to calculate the electromagnetic torque.

C. GSC MODEL

The GSC dynamic model in the direct-quadrature (DQ) rotating reference frame can be described as follows [18]:

$$\begin{aligned} v_d &= v_{id} - R i_d - L \frac{di_d}{dt} + \omega L i_q, \\ v_q &= v_{iq} - R i_q - L \frac{di_q}{dt} + \omega L i_d, \end{aligned} \tag{3}$$

where L and R denote the grid inductance and resistance, respectively; v_d and v_q denote the grid voltages in the DQ frame. i_d and i_q denote the grid currents in the DQ frame. v_{id} and v_{iq} denote the GSC voltages in the DQ frame. We assume that the d-axis of the DQ rotating reference frame is aligned with the grid voltage. Thus, the active and reactive powers from the GSC to the grid can be expressed as follows [18]:

$$\begin{aligned} P_{grid} &= \frac{3}{2} v_d i_d, \\ Q_{grid} &= \frac{3}{2} v_d i_q, \end{aligned} \tag{4}$$

where P_{grid} and Q_{grid} are the active and reactive powers, respectively. From the aforementioned assumption, the GSC active and reactive powers can be modulated independently using i_d and i_q.

D. DC-LINK VOLTAGE MODEL

A DC link is an energy buffer between the MSC and GSC. Its voltage can be described as the difference in power production between the MSC and GSC using the following equation [12]:

$$P_c = C V_{dc} \frac{dV_{dc}}{dt} = P_g - P_{grid}, \tag{5}$$

where P_g and P_{grid} denote the MSC and GSC power, respectively; P_c describes the power stored in the DC link; V_{dc} denotes the DC-link voltage; and C denotes the DC-link capacitor. According to Eq. 5, the DC-link voltage model is nonlinear.

E. ESS MODEL

ESS power model describes the ESS power and its SoC. ESS has a physical constraints that it should keep the SoC value between 0 to 1 since both values denote empty and fully charged energy, respectively. The conventional method of the ESS power output reference is defined as follows.

$$P_{ESS}^* = K_P(V_{dc}^* - V_{dc}) + \int K_I(V_{dc}^* - V_{dc}) \tag{6}$$

P_{ESS}^* denotes the ESS power reference. The above conventional ESS power reference for LVRT does not consider the ESS physical limitation and it can result in significant stability issue during LVRT operation. We handled this issue

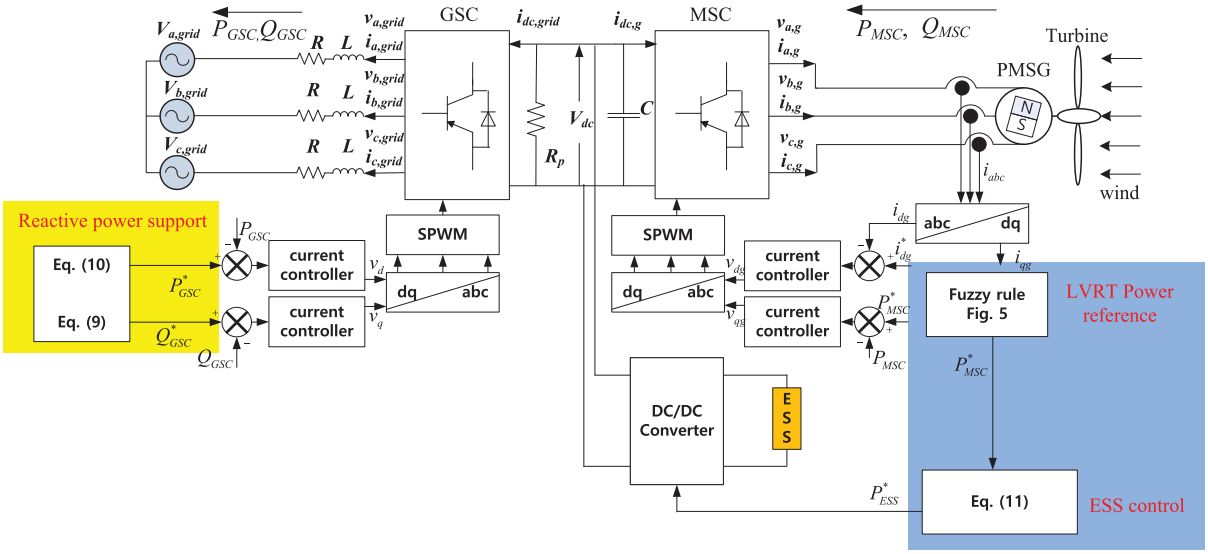

FIGURE 2. Overall control block diagram of the proposed method.

in simulation & experimental results section and we proposed a fuzzy logic control method to define proper ESS power reference by considering ESS constraint in the fuzzy logic algorithm. We described it in the following section. From the ESS power the SoC can be modelled as follows.

$$W_{ESS}(t) = \int_0^t P_{ESS}(u)du + W_{ESS}(0) \tag{7}$$

$$SoC(t) = W_{ESS}(t)/W_{Max} \tag{8}$$

W_{ESS} indicates the ESS stored energy. W_{Max} denotes the maximum ESS energy capacity.

III. PROPOSED LVRT CONTROL SYSTEM

For coordinated LVRT control between a WT and ESS, the power references of the devices are different according to their operation status at the time of a grid fault. The ESS SoC changes based on the past operations before the grid fault, and the WT rotor speed varies based on its previous operation mode and past wind speed conditions. Thus, the operation conditions of the devices are usually different at the time of a grid fault, and the LVRT power reference should be defined according to these conditions. Therefore, the power reference during a grid fault is defined using a fuzzy-logic algorithm that considers the ESS SoC and WT inertial energy capacity. Further, the MSC, which is dependent on the power reference, is controlled by regulating the DC-link voltage. The MSC and ESS operate at a specific active power level from the fuzzy-logic controller, and the GSC can produce reactive power for grid voltage restoration, independent of the MSC and ESS. The overall control structure is shown in Fig. 2.

A. GSC ACTIVE AND REACTIVE POWER REFERENCES

The required LVRT power variation should be defined before we use the fuzzy logic-controller for the MSC and ESS. The grid code requires a certain level of reactive power for grid voltage support. The required reactive power is generally proportional to the amount of grid voltage sag. Therefore, the reactive power reference for the GSC can be defined as a per-unit (pu) value, and can be expressed as the following equation:

$$\begin{aligned} I^*_{q,GSC} &= 2V_{sag}, \qquad (\text{for } I^*_{q,GSC} \le 1 \text{ pu}) \\ Q^*_{GSC} &= I^*_{q,GSC} V_d, \end{aligned} \tag{9}$$

where $I^*_{q,GSC}$ is the reactive current reference for grid voltage sag, V_{sag}. Q^*_{GSC} denotes the reactive power reference which is obtained from $I^*_{q,GSC}$ and PCC d-axis voltage, V_d. According to Eq. 9, the GSC should produce full reactive current when the voltage sag is larger than 50% and many grid codes require WPS to support reactive power as much as twice of the voltage sag during grid fault [7]. By using the reactive current reference, the active power reference of the GSC can be obtained by following equation:

$$\begin{aligned} I^*_{d,GSC} &= \sqrt{1 - (I^*_{q,GSC})^2}, \\ P^*_{GSC} &= I^*_{d,GSC} V_d, \end{aligned} \tag{10}$$

where, $I^*_{d,GSC}$ is active current reference and P^*_{GSC} denotes the active power reference. The total available current is limited by the converter capacity; thus, the active current reference is limited by the reactive current reference. The priority of the GSC control during a grid fault is reactive power production for grid support. The reactive power reference is defined according to voltage sag, and then the active power reference is defined.

B. FUZZY-LOGIC-BASED LVRT CONTROL OF MSC AND ESS

After defining a GSC power reference, the required power references for the MSC and ESS can be determined by considering the GSC active power reference and inertial response

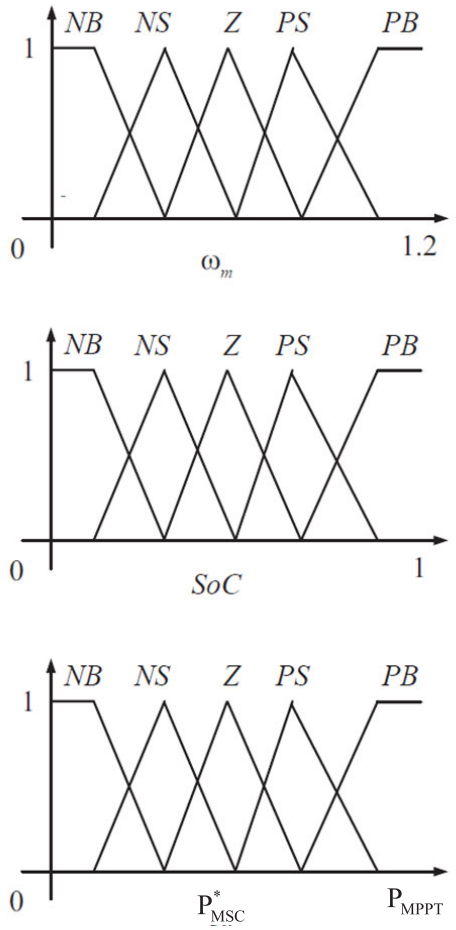

FIGURE 3. Membership functions of the proposed method.

	P^*_{MSC}				
	NB	*NS*	*Z*	*PS*	*PB*
NB	*Z*	*NS*	*NS*	*NB*	*NB*
NS	*PS*	*Z*	*NS*	*NB*	*NB*
Z	*PS*	*PS*	*Z*	*NS*	*NS*
PS	*PB*	*PB*	*PS*	*Z*	*NS*
PB	*PB*	*PB*	*PS*	*PS*	*Z*

FIGURE 4. Fuzzy rule of the proposed method.

capacity, and the ESS SoC. First, we calculate the required power reduction for LVRT using the GSC active power reference. To maintain the DC-link voltage, the sum of the MSC power and ESS discharge power should be equal to the GSC active power reference. Thus, the following relationship can be obtained:

$$P^*_{MSC} + P^*_{ESS} = P^*_{GSC}, \tag{11}$$

where P^*_{MSC} and P^*_{ESS} are the MSC and ESS discharge power references, respectively. When the grid voltage sag is larger than 50%, P^*_{GSC} becomes zero, and P^*_{MSC} and P^*_{ESS} should have the same absolute value with different signs. That is, when the grid voltage sag is larger than 50%, all the power from the MSC should be stored in the ESS to regulate the DC-link voltage as the GSC cannot produce any active power. Thus, when P^*_{MSC} is large, the ESS charge power should also be large in case of a large voltage sag ($>$ 50%). The reference value for P^*_{MSC} should be determined based on the operation status at the time of a grid fault. The fuzzy-based controller can be used for determining an appropriate value for P^*_{MSC}. The input and output membership functions should be defined for the fuzzy-logic control. We define the membership functions as shown in Fig. 3. Using these membership functions, we defined the fuzzy rule for proper power management of the MSC and ESS, as shown in Fig. 4. The overall rule based fuzzy logic controller is described in Fig 5. We defined maximum value of the WT rotor speed and ESS SoC operation ranges to 1.2 pu and 1 pu, respectively. These rotor speed and SoC membership functions are used to obtain fuzzy membership values, $\mu(\omega_m)$ and $\mu(SoC)$. We used Takagi-Sugeno method for defuzzification by using membership function of P^*_{MSC}. After the defuzzifier, the MSC power reference can be obtained from its membership value as described in Fig. 5. Therefore, we defined the fuzzy rule so that the burden of LVRT is divided between the WT and ESS, thereby resulting in reliable reserve power management.

IV. SIMULATION AND EXPERIMENTAL RESULTS

In this study, we validated the effectiveness of the proposed method using the MATLAB/Simulink SimPowerSystems toolbox. After obtaining simulation results, we also validated the proposed method in real time simulation using Scalexio. The overall system parameters are presented in Table 1 for validation. We compared the performance of the proposed method during an 80% grid voltage sag, which means that the GSC should produce full reactive power and no active power. The three phase voltages at the PCC during grid fault are described in Fig. 6 and the d-axis voltage in dq synchronous frame is described in Fig. 7. The grid fault is occurred at 1 second and grid voltage is reduced its value to 20% of its nominal value. In this case, the PMSG WT should reduce its active power production to zero using the MSC and ESS LVRT controls. The conventional methods regulate the DC link in the MSC and ESS, whereas the proposed method uses fuzzy-based LVRT. In case of conventional method, we used PI control method for DC link voltage regulation. More advanced nonlinear control can be used to regulate DC link voltage. However, it is hard work to find proper control gain for satisfying both transient and stability performance even in case of applying advanced nonlinear control. To evaluate

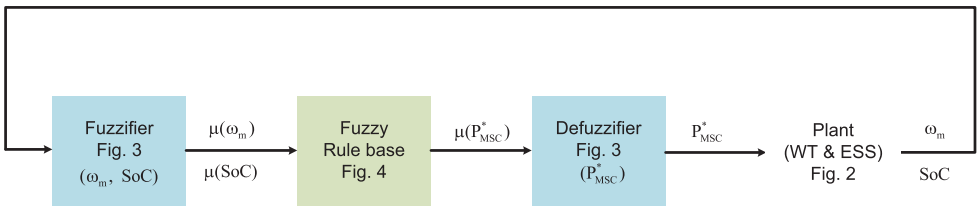

FIGURE 5. Fuzzy logic controller.

TABLE 1. System parameters used in simulation.

Parameter	Value	Unit
Rated power	1.63	MW
Rated wind speed	12	m/s
Max. power coefficient	0.5	
Optimal tip speed ratio	9.9495	
Blade radius	33.05	m
Air density	1.12	kg/m^3
Max. rotor speed	4.335	rad/sec
DC-link voltage	1150	V
Turbine inertia	6500	kgm^2
ESS Capacity	1	kWh

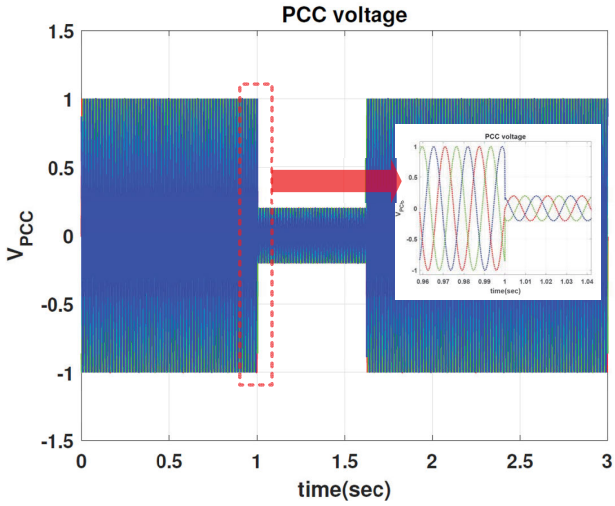

FIGURE 6. PCC three phase voltages during a balanced voltage sag (80%) (case 1 & 2).

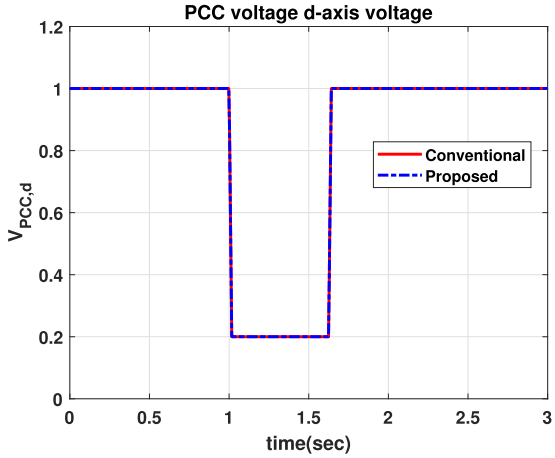

FIGURE 7. PCC d axis voltage during a balanced voltage sag (80%) (case 1 & 2).

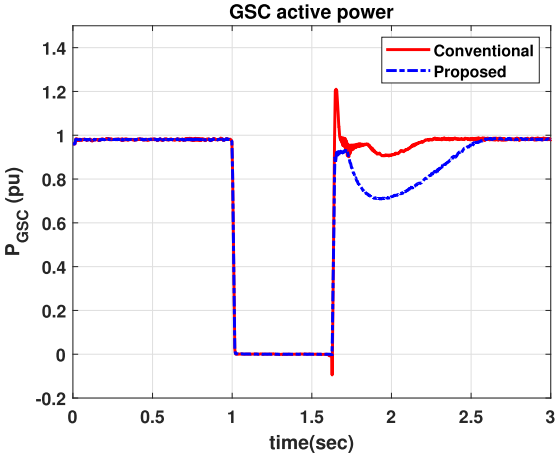

FIGURE 8. Grid active power during a balanced voltage sag (80%) (case 1).

the effectiveness of the proposed method, we considered the case when the ESS SoC approaches its maximum value, and no additional LVRT controls are available in the conventional method.

The proposed method effectively handles this situation with efficient power management of the WT and ESS during a grid fault.

A. CASE 1: ESS SoC REACHES ITS MAXIMUM VALUE

To highlight the effectiveness of the proposed method, we considered a case with the ESS SoC limit violation, which can occur in a conventional method. The ESS effectively mitigates the DC-link voltage variation during grid faults; thus, there is a significant problem in DC-link regulation when the ESS SoC approaches its limit. In Fig. 8, the grid active power was reduced to zero to produce full reactive power. As the grid fault has an 80% voltage sag, the reactive power can be 0.2 pu for the full reactive current (1 pu reactive current) as shown in Fig. 9. Figure 10 and Fig. 11 illustrate active and reactive currents during the grid fault, respectively. Since the q-axis voltage is zero, d-axis current is the active

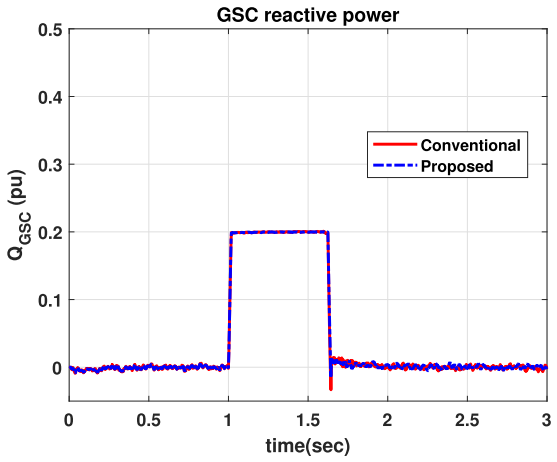

FIGURE 9. Grid reactive power during a balanced voltage sag (80%) (case 1).

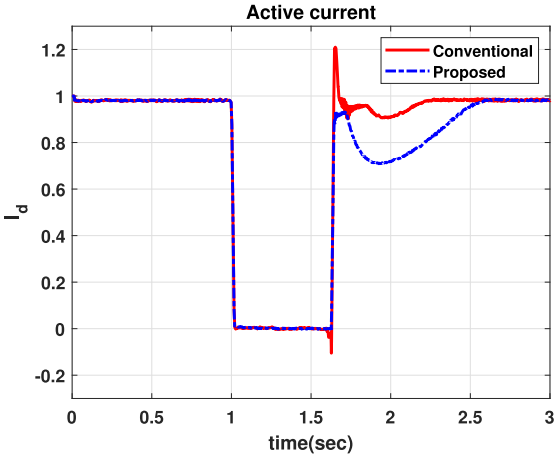

FIGURE 10. PCC d-axis (active) current during a balanced voltage sag (80%) (case 1).

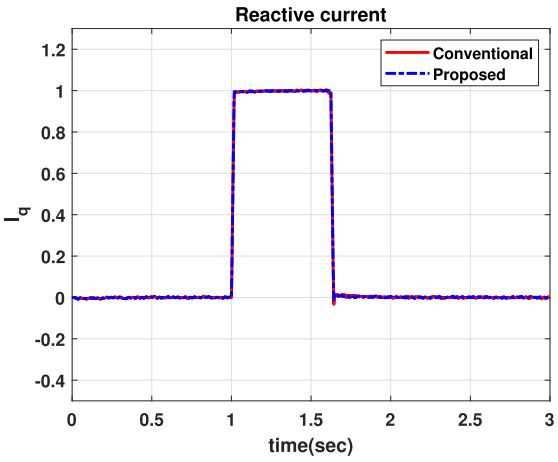

FIGURE 11. PCC q-axis (reactive) current during a balanced voltage sag (80%) (case 1).

current and q-axis current is reactive current. Thus, d-axis current is similar with grid active power curve. Reactive current is similar with reactive power curve. Since the voltage

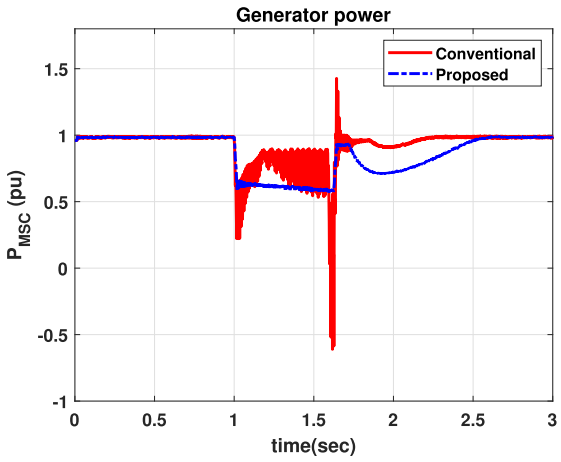

FIGURE 12. Generator active power during a balanced voltage sag (80%) (case 1).

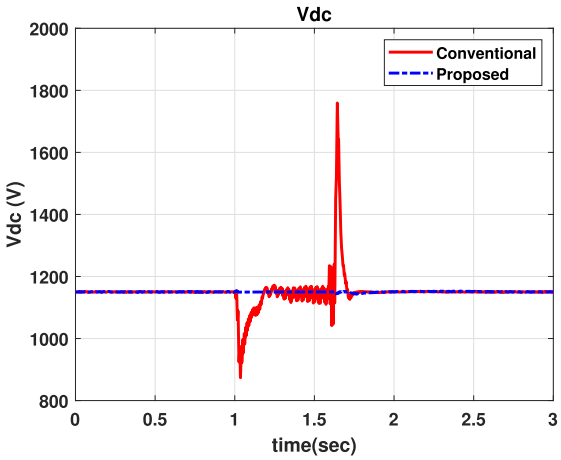

FIGURE 13. DC-link voltage during a balanced voltage sag (80%) (case 1).

is 0.2 pu during the grid fault, the reactive power is only 0.2 pu even though the reactive current is as high as 1 pu during the grid fault. In the proposed method, the generator power has less power production as compared to that of the conventional method, as shown in Fig. 12. By considering the ESS SoC and WT rotor speed, the effective power reference values were evaluated from the proposed method. The GSC active and reactive powers obtained from the two methods had similar responses; with the only difference being that the GSC active power had a slightly larger value in the conventional method immediately after the grid fault occurred, because of the DC-link voltage, as shown in Fig. 13. As the GSC is controlled to regulate the DC-link voltage when the grid fault is cleared, the GSC produces a large amount of active power to reduce the DC-link voltage. The DC-link voltage increased because the ESS failed to regulate it when the SoC approached its maximum value, as shown in Fig. 16. The ESS SoC violated its limit because its charging reference is determined by DC-link voltage variation and there is no consideration about the ESS reserve capacity in the conven-

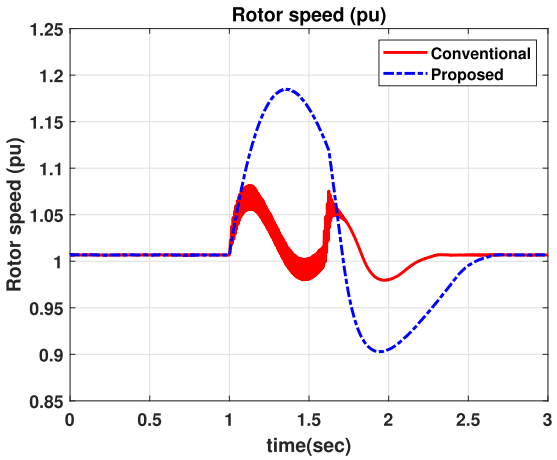

FIGURE 14. Rotor speed variation during a balanced voltage sag (80%) (case 1).

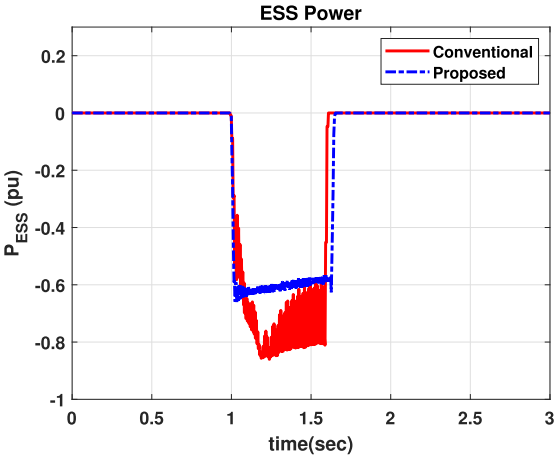

FIGURE 15. ESS power during a balanced voltage sag (80%) (case 1).

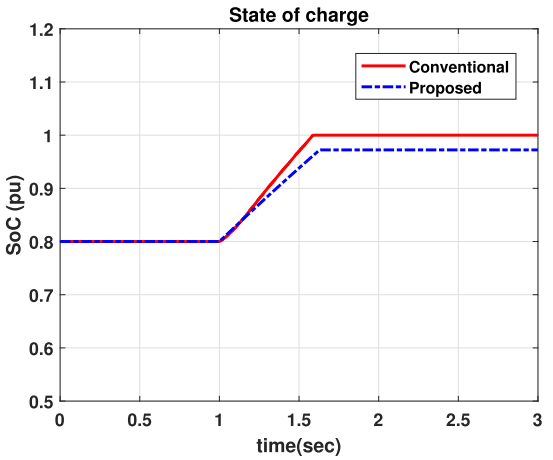

FIGURE 16. SoC during a balanced voltage sag (80%) (case 1).

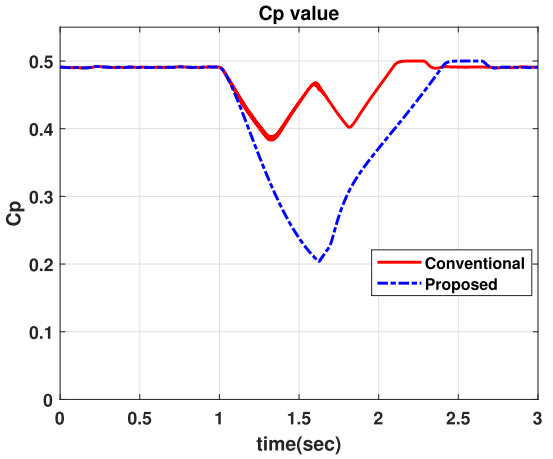

FIGURE 17. Power coefficient during a balanced voltage sag (80%) (case 1).

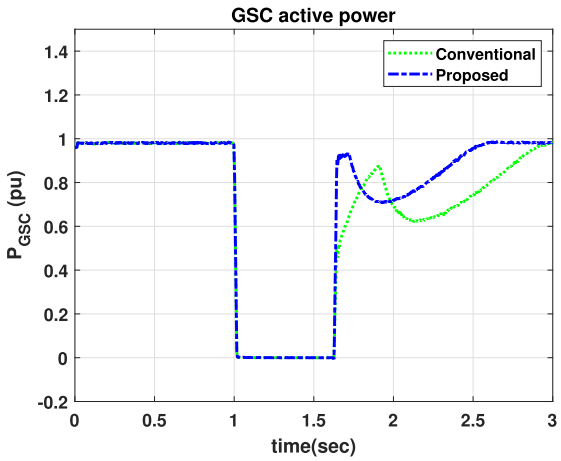

FIGURE 18. Grid active power during a balanced voltage sag (80%) (case 2).

tional method. Figure 15 describes ESS output power. ESS power is controlled to take a part of LVRT burden. Negative value means that ESS charges power to regulated dc link voltage. Different rotor speeds that do not violate constraints are shown in Fig. 14. The rotor speed of the conventional method had a smaller value as compared to that of the proposed method. In the conventional method, the MSC and ESS failed to appropriately divide the burden of LVRT operations when the SoC approached its limit. Furthermore, the power coefficient had different profiles for various rotor speeds, as shown in Fig. 17.

B. CASE 2: ROTOR SPEED LIMIT VIOLATION

We also considered the case when the rotor speed violation occurs to highlight the effectiveness of the proposed method compared to conventional method. In this case, the rotor speed violation can result in a mechanical component problem and reduce its life span. Compared to the previous case study, the DC-link voltage was regulated efficiently in conventional method. However, it resulted in mechanical stress because of rotor speed violation and it produced worse performance in DC-link voltage regulation as compared to that by the proposed method because the burden of LVRT

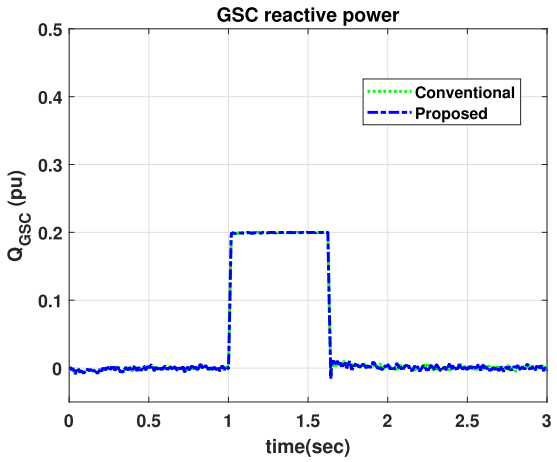

FIGURE 19. Grid reactive power during a balanced voltage sag (80%) (case 2).

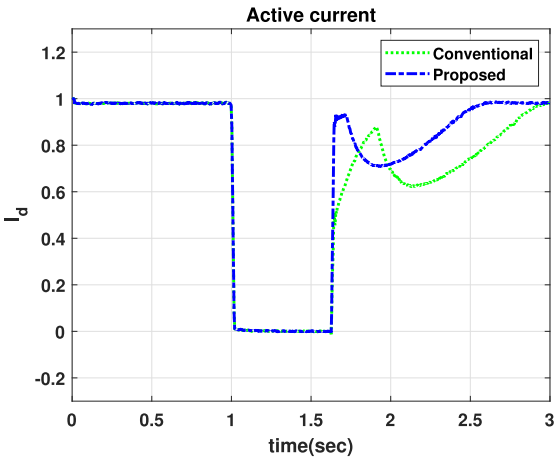

FIGURE 20. PCC d axis voltage during a balanced voltage sag (80%) (case 2).

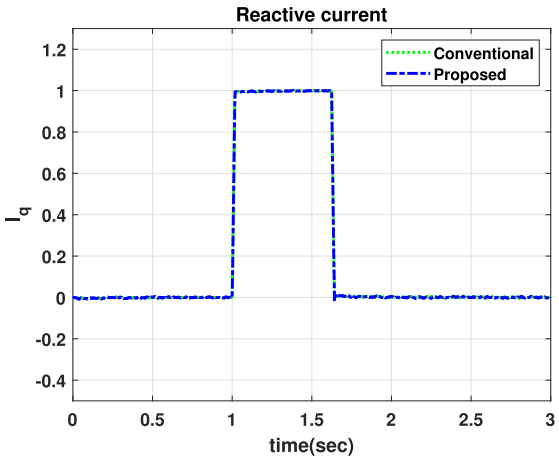

FIGURE 21. PCC d axis voltage during a balanced voltage sag (80%) (case 2).

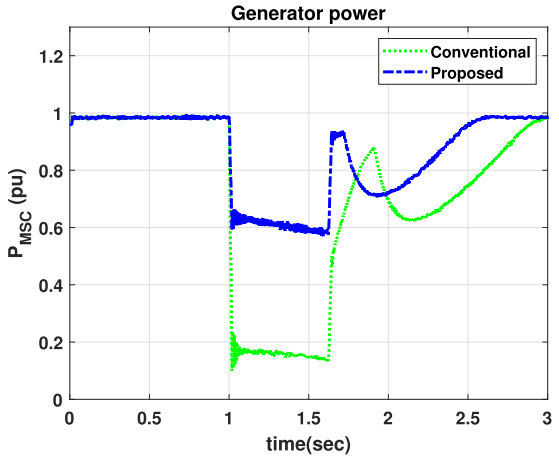

FIGURE 22. Generator active power during a balanced voltage sag (80%) (case 2).

operation was not proper. In Fig. 18, the grid active power is reduced to zero to produce full reactive power. As the grid fault has an 80% voltage sag, the reactive power can be obtained as 0.2*pu* for the full reactive current (1*pu* reactive current) as shown in Fig. 19. Figure 20 and Fig. 21 illustrate active and reactive currents during the grid fault, respectively. Active current was reduced its value during the grid fault to reduce the active power from GSC and reactive current was increased to support reactive power to the grid during the grid fault. The GSC active and reactive powers of the two methods had similar responses. However, the generator active power was significantly reduced in the conventional method, as shown in Fig. 22. This can occur when the DC-link voltage controller gain in the MSC is high. Consequently, the MSC reduced its power excessively at the time of the grid fault, thereby resulting in poor DC-link regulation at that moment, as shown in Fig. 23. Moreover, the rotor speed in the conventional method violated the constraints, as shown in Fig. 24. Figure 25 describes ESS output power. In this case, the ESS charged less power in conventional method since WT reduced large power taking almost burden of the LVRT. It resulted in reduced burden in the ESS. It increased up to nearly 1.45 *pu* during the grid fault, which can induce severe mechanical problems. The ESS SoCs of both methods had less values than its limit, as shown in Fig. 26. Furthermore, the power coefficient had different profiles for various rotor speeds, as shown in Fig. 27. In this case the conventional method had less power coefficient value because it used large inertial power during the fault. We considered 80% voltage in this paper. If the voltage sag is 50% it is same condition since grid codes require same reactive power current (100%) from wind power system. If the voltage sag is less than 50%, the burden of LVRT is getting less than that of 50% voltage sag. Thus, WT can take overall LVRT burden without the need of the ESS LVRT control.

C. EXPERIMENTAL RESULTS

We investigated the performance of the proposed method in real time experimental environment. We used Scalexio which is developed by DSPACE. The WP and ESS

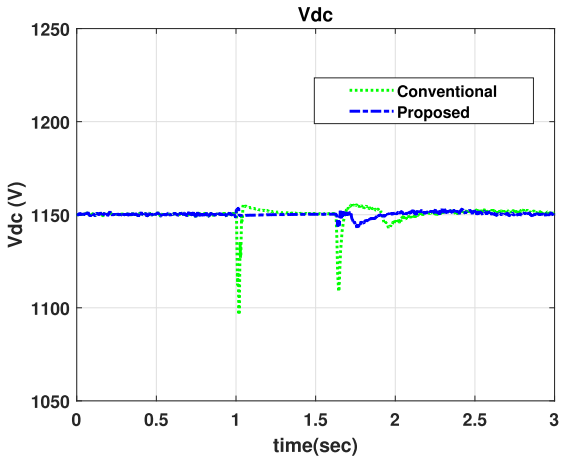

FIGURE 23. DC-link voltage during a balanced voltage sag (80%) (case 2).

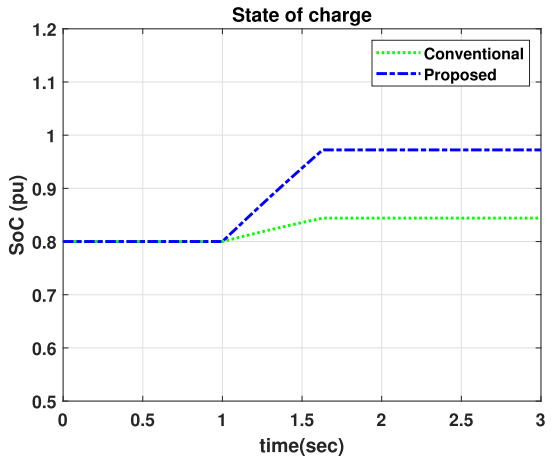

FIGURE 26. SoC during a balanced voltage sag (80%) (case 2).

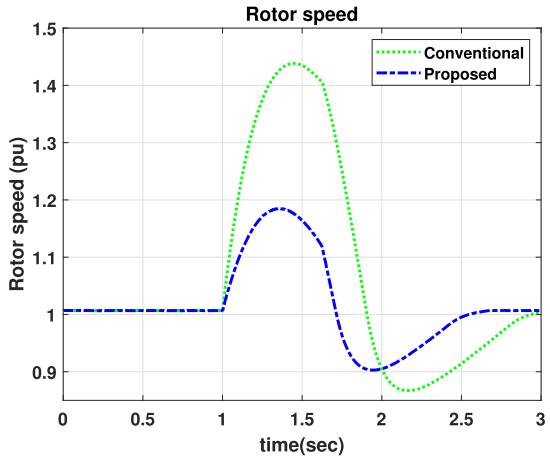

FIGURE 24. Rotor speed variation during a balanced voltage sag (80%) (case 2).

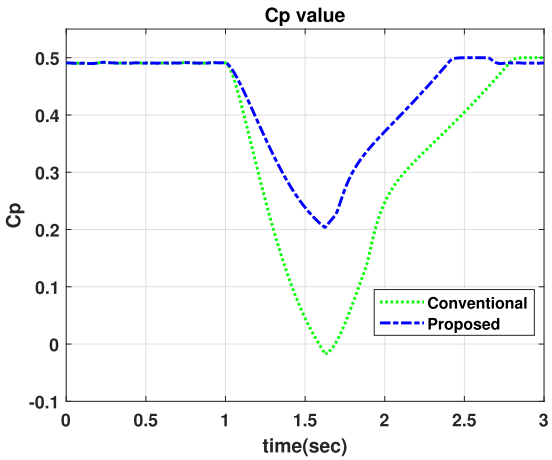

FIGURE 27. Power coefficient during a balanced voltage sag (80%) (case 2).

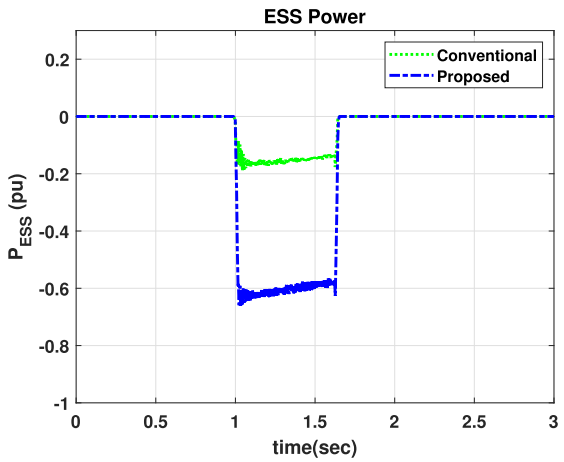

FIGURE 25. ESS power during a balanced voltage sag (80%) (case 2).

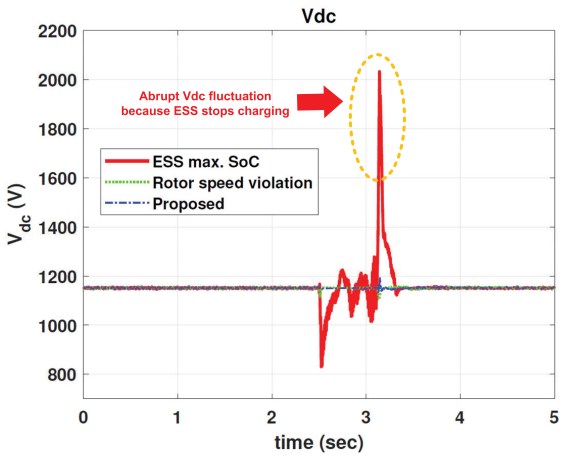

FIGURE 28. DC-link voltage during a balanced voltage sag (80%) (experimental results).

integrated power system model is simulated in Scalexio and we compared the results with the simulation results of the case studies. The sampling frequency of real time simulation is 50 kHz. Using the real-time simulation, we validated the performance of the proposed method without any issues about real time computation. In Fig. 28, the dc link voltages

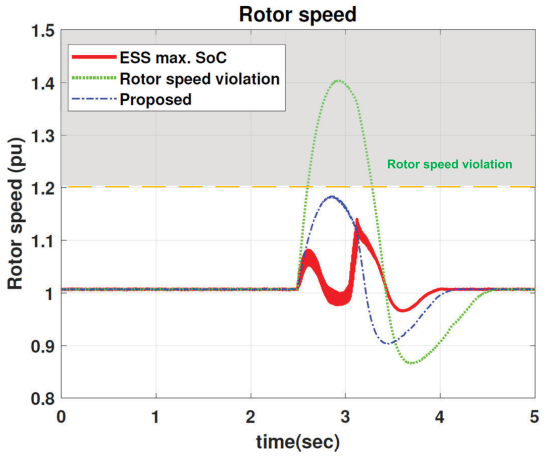

FIGURE 29. Rotor speed variation during a balanced voltage sag (80%) (experimental results).

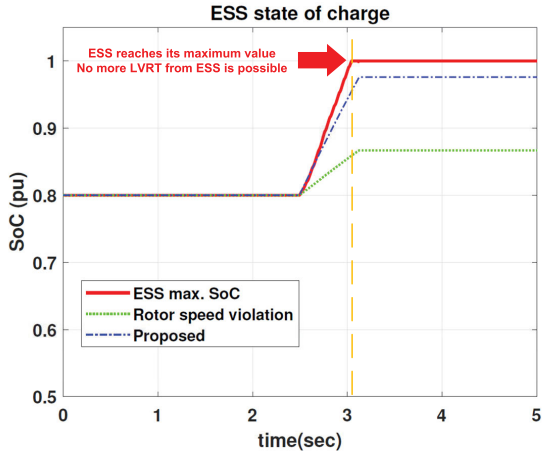

FIGURE 30. SoC during a balanced voltage sag (80%) (experimental results).

of the three cases are described. Overall tendency of the dc link voltages is similar with the simulation results and the case when ESS reaches its maximum SoC value has the worst response among three cases. The transient performance can be improved by using more advanced control algorithm, the poor response due to the SoC constraint cannot be improved without solving energy perspective problem. Figure 29 illustrated rotor speeds of the three cases. Conventional method can result in these rotor speed violation issue even though it does not have ESS SoC constraint problem as illustrated in Fig. 30. Therefore, the conventional method which is formulated in dc link regulation can result in stability problem due to these ESS SoC and WT rotor speed constraints. Moreover, it is difficult to find the proper control gains considering the system parameter variations. By accounting these constraints during LVRT control in terms of fuzzy logic algorithm, the proposed method can effectively improve the LVRT response without constraints violation.

V. CONCLUSION

In this study, we proposed a coordinated fuzzy-based LVRT method that considers the inertial response capabilities of a WT and an ESS SoC. Previous studies have focused on the ESS LVRT control for regulating the DC-link voltage during a grid fault. However, an ESS can have different SoC values when a grid fault occurs. The DC-link voltage can vary significantly when an ESS approaches its SoC limit before the grid fault is cleared. Thus, it is important to coordinate the LVRT control between the WTs and ESSs during a grid fault. We devised a fuzzy-based LVRT control method in part by considering the LVRT capability of the WT and ESS. Using the proposed method, the LVRT control burden was divided between the WT and ESS, as illustrated by the simulation results. Thus, the LVRT control method was successfully implemented without violating the constraints on either devices. As demonstrated by the simulation results, the proposed method was more reliable as compared to the conventional method. Using the proposed method, the required ESS reserve capacity can be effectively reduced as the WT inertial response considers the maximum rotor speed limit. The proposed fuzzy-logic-based LVRT method can be easily applied to a WT with constraints and other control objectives. To validate the effectiveness of the proposed method, we considered case studies on SoC limit and rotor speed violations during a grid fault using MATLAB/Simulink SimPowerSystems considering a topological circuit model. We also validated the results using Scalexio for real-time simulation. From simulation and experiment results, we confirmed that the proposed method can help achieve the successful LVRT operation in energy management between the WT and ESS, and even improve the DC-link voltage regulation. Further research could include the WT and ESS coordinated fuzzy control method for handling frequency fluctuation and its stability impact. It can be expected that it can effectively solve this issue in terms of operation reliability of the WT and ESS.

REFERENCES

[1] H. Polinder, F. F. A. Van Der Pijl, G.-J. De Vilder, and P. J. Tavner, "Comparison of direct-drive and geared generator concepts for wind turbines," *IEEE Trans. Energy Convers.*, vol. 21, no. 3, pp. 725–733, Sep. 2006.

[2] M. Chinchilla, S. Arnaltes, and J. C. Burgos, "Control of permanent-magnet generators applied to variable-speed wind-energy systems connected to the grid," *IEEE Trans. Energy Convers.*, vol. 21, no. 1, pp. 130–135, Mar. 2006.

[3] C. Kim, Y. Gui, and C. C. Chung, "Maximum power point tracking of a wind power plant with predictive gradient ascent method," *IEEE Trans. Sustain. Energy*, vol. 8, no. 2, pp. 685–694, Apr. 2017.

[4] Y. Gui, X. Wang, F. Blaabjerg, and D. Pan, "Control of grid-connected voltage-source converters: The relationship between direct-power control and vector-current control," *IEEE Ind. Electron. Mag.*, vol. 13, no. 2, pp. 31–40, Jun. 2019.

[5] J. Kim, E. Muljadi, V. Gevorgian, and A. F. Hoke, "Dynamic capabilities of an energy storage-embedded DFIG system," *IEEE Trans. Ind. Appl.*, vol. 55, no. 4, pp. 4124–4134, Jul. 2019.

[6] C. Kim, E. Muljadi, and C. Chung, "Coordinated control of wind turbine and energy storage system for reducing wind power fluctuation," *Energies*, vol. 11, no. 1, p. 52, Dec. 2017.

[7] M. Tsili and S. Papathanassiou, "A review of grid code technical requirements for wind farms," *IET Renew. Power Generat.*, vol. 3, no. 3, pp. 308–332, Sep. 2009.

[8] G. Saccomando, J. Svensson, and A. Sannino, "Improving voltage disturbance rejection for variable-speed wind turbines," *IEEE Trans. Energy Convers.*, vol. 17, no. 3, pp. 422–428, Sep. 2002.
[9] A. Mullane, G. Lightbody, and R. Yacamini, "Wind-turbine fault ride-through enhancement," *IEEE Trans. Power Syst.*, vol. 20, no. 4, pp. 1929–1937, Nov. 2005.
[10] J. Matas, M. Castilla, J. M. Guerrero, L. G. de Vicuna, and J. Miret, "Feedback linearization of direct-drive synchronous wind-turbines via a sliding mode approach," *IEEE Trans. Power Electron.*, vol. 23, no. 3, pp. 1093–1103, May 2008.
[11] J. F. Conroy and R. Watson, "Low-voltage ride-through of a full converter wind turbine with permanent magnet generator," *IET Renew. Power Gener.*, vol. 1, no. 3, pp. 182–189, Sep. 2007.
[12] K.-H. Kim, Y.-C. Jeung, D.-C. Lee, and H.-G. Kim, "LVRT scheme of PMSG wind power systems based on feedback linearization," *IEEE Trans. Power Electron.*, vol. 27, no. 5, pp. 2376–2384, May 2012.
[13] S. Alepuz, A. Calle, S. Busquets-Monge, S. Kouro, and B. Wu, "Use of stored energy in PMSG rotor inertia for low-voltage ride-through in back-to-back NPC converter-based wind power systems," *IEEE Trans. Ind. Electron.*, vol. 60, no. 5, pp. 1787–1796, May 2013.
[14] W. Wang, B. Ge, D. Bi, M. Qin, and W. Liu, "Energy storage based LVRT and stabilizing power control for direct-drive wind power system," in *Proc. Int. Conf. Power Syst. Technol.*, Oct. 2010, pp. 1–6.
[15] J. Liu, W. Yao, J. Fang, J. Wen, and S. Cheng, "Stability analysis and energy storage-based solution of wind farm during low voltage ride through," *Int. J. Electr. Power Energy Syst.*, vol. 101, pp. 75–84, Oct. 2018.
[16] J. Yao, J. Li, L. Guo, R. Liu, and D. Xu, "Coordinated control of a hybrid wind farm with PMSG and FSIG during asymmetrical grid fault," *Int. J. Electr. Power Energy Syst.*, vol. 95, pp. 287–300, Feb. 2018.
[17] J. Li, N. Wang, D. Zhou, W. Hu, Q. Huang, Z. Chen, and F. Blaabjerg, "Optimal reactive power dispatch of permanent magnet synchronous generator-based wind farm considering levelised production cost minimisation," *Renew. Energy*, vol. 145, pp. 1–12, Jan. 2020.
[18] M. E. Haque, M. Negnevitsky, and K. M. Muttaqi, "A novel control strategy for a variable speed wind turbine with a permanent magnet synchronous generator," in *Proc. IEEE Ind. Appl. Soc. Annu. Meeting*, Oct. 2008, pp. 1–8.

CHUNGHUN KIM (Member, IEEE) received the B.S. degree in electronic electricity computer engineering and the unified M.S. and Ph.D. degrees in electrical engineering from Hanyang University, Seoul, South Korea, in 2011 and 2018, respectively. In 2017, he was a Visiting Scholar with the National Renewable Energy Laboratory, Golden, CO, USA. In 2018, he was a Postdoctoral Researcher with the Department of Electrical Engineering, Kyungpook National University, Deagu, South Korea, where he was a Research Professor, in 2019. He is currently an Assistant Professor with the Department of AI Electrical Engineering, Pai Chai University, Daejeon, South Korea. His current research interests include integration of renewable energy and optimization of distributed energy resource in micro-grid.

WONHEE KIM (Member, IEEE) received the B.S. and M.S. degrees in electrical and computer engineering and the Ph.D. degree in electrical engineering from Hanyang University, Seoul, South Korea, in 2003, 2005, and 2012, respectively. From 2005 to 2007, he was with Samsung Electronics Company, Suwon, South Korea. In 2012, he was with the Power and Industrial Systems Research and Development Center, Hyosung Corporation, Seoul. In 2013, he was a Postdoctoral Researcher with the Institute of Nano Science and Technology, Hanyang University. He was also a Visiting Scholar with the Department of Mechanical Engineering, University of California, Berkeley, CA, USA. From 2014 to 2016, he was with the Department of Electrical Engineering, Dong-A University, Busan, South Korea. He is currently an Associate Professor with the School of Energy Systems Engineering, Chung-Ang University, Seoul. His current research interests include nonlinear control and nonlinear observers and their industrial applications.